Matching color images: the effects of axial chromatic aberration

David H. Marimont

Xerox Palo Alto Research Center, 3333 Coyote Hill Road, Palo Alto, California 94304

Brian A. Wandell

Department of Psychology, Stanford University, Stanford, California 94305

We show how to compute and to use the wavelength-dependent optical transfer function (OTF) to create color matches between spatially patterned images. We model the human OTF as a defocused optical system with a circular aperture. In our model the defocus arises from axial chromatic aberration and wavelength-independent aberrations. From the computed OTF it is apparent that high-spatial-frequency components of the image can play little role in contrast and color appearance and that in the spatial-frequency range from 5 to 20 cycles/deg the visual system is dichromatic, because there is no contrast in the short-wavelength receptor signal. We show how to use the wavelength-dependent OTF to match color images across displays by setting matches in corresponding spatial-frequency bands. Because chromatic aberration so affects the OTF, this new procedure is a significant improvement over the conventional procedure of setting matches point by point.

1. INTRODUCTION

Color-matching experiments play an important role in both basic color science and applications of color science. Color-matching experiments are the key behavioral experiments that define the relationship between the initial encoding of light by the photopigments and the physiological response of the photoreceptors.[1,2] The experiments are also an essential component of the industrial standards of color-image representation.[3]

The color-matching experiments used to define the properties of the encoding of light in the CIE's 1931 and 1964 standards are based on relatively large uniform fields. When we restrict our analysis of the photoreceptor absorptions to large uniform fields, we can avoid the effects of axial chromatic aberration for color matching. When we begin to consider matches between images with spatial patterns, however, we must consider the effects of axial chromatic aberration, the largest ocular aberration.

Our main purpose in this paper is to consider the implications of axial chromatic aberration for color matching. Axial chromatic aberration causes a different amount of defocus for each wavelength incident at the cornea. Because axial chromatic aberration involves both the wavelength and the spatial pattern of the image, it blurs the line dividing the fields of color and pattern vision, and it requires a joint treatment of pattern and color.

We report on our study of how axial chromatic aberration influences the photoreceptor absorptions of patterned stimuli, such as the images on color displays. We describe our analysis of the effects of chromatic aberration on the basic CIE colorimetric standards for establishing color matches across different display media.

In the pages that follow, we describe a collection of methods to clarify how axial chromatic aberration transforms the corneal image into a retinal image. We base our calculations on an analysis of the chromatic aberration of a diffraction-limited optical system with a circular aperture described by Hopkins.[4] We implement Hopkins's calculation, which uses the parameters of the human eye,[5–11] and we use the results of Williams *et al.*[12] to incorporate the wavelength-independent aberrations. We have tried to understand the effects of axial chromatic aberration by considering a series of graphical characterizations of the system transformation and by examining the consequences of axial chromatic aberration for several test stimuli.

A. Main Theoretical Result

Conventional colorimetric practice is to establish color matches between uniform fields by equating the effects of the two displays on the photoreceptors. A principal result of colorimetry is that when we match two images on emissive displays, such as two television monitor images, the primary intensities needed for matching across two displays are related by a linear transformation (represented by a 3 × 3 matrix).

In current practice one generalizes color matching from uniform fields to patterned fields by establishing point-by-point matches between the two images. This generalization of the color-matching procedure is incorrect, because it fails to account adequately for the effect of axial chromatic aberration on the formation of the *retinal* image. The main difficulty with this procedure is that axial chromatic aberration blurs the retinal images of image points, and the amount of blurring may differ for corresponding points from the two images. Hence matching images point by point is not in general equivalent to matching *retinal* images point by point.

We show that the correct procedure is to transform the display primary images into the spatial-frequency do-

main. To the extent that the optics of the eye acts as a shift-invariant linear system, the sinusoidal components in the displays will also be imaged as sinusoidal components. When we represent the display primary images as sums of spatial frequencies, rather than sums of points, the simple color-matching rules generalize properly. The amplitudes of the spatial-frequency components of the three primaries needed for matching across the two displays are related by a linear transformation that depends on spatial frequency. The linear transformation between the intensities of the uniform images is simply a special case.

B. Overview

In Section 2 we describe our implementation of axial chromatic aberration. In Section 3 we introduce several graphic methods of illustrating the effects of chromatic aberration on the formation of the retinal image, incorporate the effects of wavelength-independent aberrations on the retinal image, and analyze the effects of chromatic aberration on photopigment absorptions. In Section 4 we describe the implications of our analysis for the practical problem of equating images displayed on devices that have different emissive primaries.

2. METHODS

A. Optical Transfer Function of the Model Eye

Hopkins[4] calculated the optical transfer function (OTF) of a defocused system with a circular aperture. He assumed a defocused system with no other aberrations. His formula expresses the OTF as a function of reduced spatial frequency s, defocus w_{20}, and wavelength λ. Hopkins showed that the OTF is circularly symmetric and thus can be characterized with use of one-dimensional patterns. Correspondingly, in the spatial-frequency domain we can define the OTF as a function of a single spatial-frequency parameter, the reduced spatial frequency, which ranges from 0 to 2. (The upper limit defines the diffraction-limited spatial-frequency cutoff.) The variable w_{20} is a measure of defocus with respect to optical path length error. The variable λ is the wavelength of the incident light. We refer to the Hopkins OTF as $H(s; \lambda, w_{20})$. (See Table 1 for definitions of mathematical symbols used in this paper.)

Hopkins's formula for the OTF is

$$H(s; \lambda, w_{20})$$
$$= \frac{4}{\pi a} \int_0^{\sqrt{1-(s/2)^2}} \sin\left[a\left(\sqrt{1 - y^2} - |s|/2\right) \right] dy, \quad (1)$$

where

$$a = \frac{4\pi}{\lambda} w_{20}|s|.$$

We can use this form of the OTF for numerical computation. Hopkins also showed, however, that the formula can be integrated in closed form (see Appendix A).

Two aspects of Hopkins's formulation are inconvenient for our calculations. First, we prefer to express the frequency variable in terms of cycles per degree ν rather

than in terms of the reduced spatial frequency. We convert from reduced spatial frequency to cycles per degree by using the formula

$$s = c \frac{\lambda}{D_0 p} \nu, \quad (2)$$

where c is degrees per meter for the human eye, D_0 is the dioptric power of the unaccommodated eye, and p is the radius of the entrance pupil in meters. This relationship is derived in Appendix B.

Second, because empirical measurements of defocus caused by axial chromatic aberration are reported in terms of diopters, we need an expression to relate relative defocus in diopters, $D(\lambda)$, and the variable w_{20}. We use the formula

$$w_{20}(\lambda) = \frac{p^2}{2} \frac{D_0 D(\lambda)}{D_0 + D(\lambda)}. \quad (3)$$

This relationship is derived in Appendix C. At the in-focus wavelength, $D(\lambda) = 0$, so $w_{20} = 0$, as well.

Table 1. Definitions of Mathematical Symbols

|	
s	Reduced spatial frequency
λ	Wavelength in meters
w_{20}	Optical path length error
$H(s; \lambda, w_{20})$	Hopkins OTF
p	Radius of entrance pupil in meters
c	Degrees per meter for the human eye
ν	Spatial frequency in cycles per degree
D_0	Dioptric power of the eye at in-focus wavelength
$D(\lambda)$	Relative defocus of the eye as a function of wavelength
q_1, q_2, q_3	Parameters relating defocus in diopters to wavelength
x	Spatial location in degrees of visual angle
$f(x, \lambda), F(\nu, \lambda)$	Corneal image and Fourier transform in x
$g(x, \lambda), G(\nu, \lambda)$	Retinal image and Fourier transform in x
$o_m(x, \lambda), O_m(\nu, \lambda)$	Impulse response and OTF for Hopkins's model
$O_d(\lambda)$	Diffraction-limited OTF (at the in-focus wavelength)
$K(\nu)$	Scale factor that models wavelength-independent aberrations
$o(x, \lambda), O(\nu, \lambda)$	Impulse response and OTF for combined model
$A_i(\lambda)$	Absorption curve of ith photopigment
$R_i(\nu, \lambda)$	Wavelength sensitivity of ith photopigment, measured through optics
W	Range of visual wavelengths
$P_i(\nu)$	Fourier-transform spatial pattern of ith photopigment absorptions
$M_j(\lambda)$	SPD of jth display primary
$f_m(x, \lambda), F_m(\nu, \lambda)$	Display image and Fourier transform in x
$s_j(x), S_j(\nu)$	Spatial pattern of jth display primary and Fourier transform
$C_{ij}(\nu)$	Scaled OTF from jth display primary to ith photopigment
$\mathbf{P}_\nu$	Vector whose ith entry is $P_i(\nu)$
$\mathbf{S}_\nu$	Vector whose jth entry is $S_j(\nu)$
$\mathbf{C}_\nu$	Matrix whose ijth entry is $C_{ij}(\nu)$
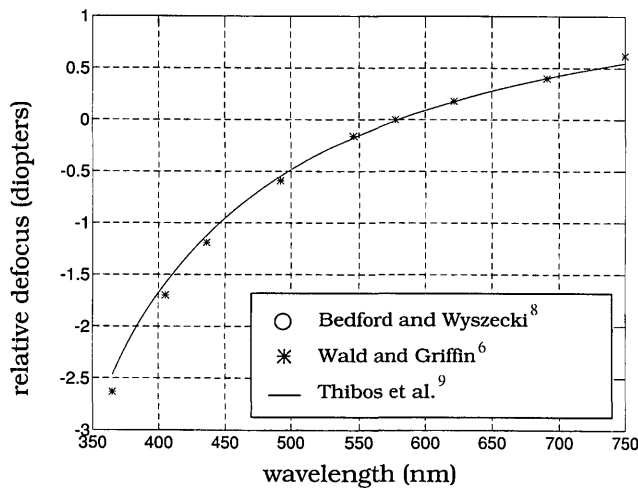
Fig. 1.   Defocus as a function of wavelength.

Finally, we use a formula derived by Thibos et al.[9] to calculate the relationship between defocus in diopters and wavelength. They express defocus by using the equation

$$D(\lambda) = q_1 - \frac{q_2}{\lambda - q_3}, \qquad (4)$$

where λ is wavelength in micrometers and $D(\lambda)$ is defocus in diopters. The values for the parameters that we use are $q_1 = 1.7312$, $q_2 = 0.63346$, and $q_3 = 0.21410$, which imply an in-focus wavelength of 580 nm. (The value for q_1 differs slightly from that used by Thibos et al.,[9] because those authors used an in-focus wavelength of 589 nm.) We plot the data from Wald and Griffin[6] and from Bedford and Wyszecki,[8] along with the predicted curve, in Fig. 1 (see also Fig. 6 of Thibos et al.[9] and Ref. 13).

Hopkins's equations permit us to calculate the OTF of a defocused optical system. We use Eq. (2) to convert spatial frequency ν to reduced spatial frequency s. We convert wavelength to relative defocus [Eq. (4)] and then to w_{20} [Eq. (3)]. The reduced spatial frequency w_{20} and wavelength are all that is required for use of Hopkins's original formula [Eq. (1)]. We call the OTF for retinal image formation $O_m(\nu, \lambda)$.

B. Computing Retinal Images

We can use the OTF to compute one-dimensional retinal images as follows. We denote the one-dimensional corneal image $f(x, \lambda)$, where x is the spatial position (degrees of visual angle) and λ is wavelength (meters). We denote the corresponding retinal image $g(x, \lambda)$. We denote the Fourier transform of these images with respect to the spatial variable x, using capital letters, $F(\nu, \lambda)$ and $G(\nu, \lambda)$.

The OTF O_m relates the Fourier transform of the corneal image, $F(\nu, \lambda)$, to the Fourier transform of the retinal image, $G(\nu, \lambda)$, by means of

$$G(\nu, \lambda) = F(\nu, \lambda)O_m(\nu, \lambda).$$

We can also perform the calculation in the space domain, using the convolution operation. We use $o(x, \lambda)$ to denote the inverse Fourier transform of the OTF. The corneal and retinal images are related by

$$g(x, \lambda) = f(x, \lambda) * o(x, \lambda),$$

where $*$ denotes convolution in the spatial variable. The function $o(x, \lambda)$ is the line-spread function of the optical system.

C. Selection of Constants

The computations that we report are all based on a few fixed constants. The values for c and D_0 are taken from Wyszecki and Stiles.[3] The value for c, 3434.07, comes from their Table 2(2.4.1); it is the multiplicative inverse of meters per degree. The value for D_0, 59.9404, comes from their Table 1(2.4.1); it is the dioptric power of the unaccommodated eye, for the full theoretical eye of LeGrand.

3. RESULTS

A. Optical Transfer Function

We have calculated the OTF's in the range of visual wavelengths according to the methods of Section 2. Figure 2 collects the resulting OTF at each wavelength into a single surface plot; two views of this plot are shown. The two dimensions of the plot are the spatial frequency of the image and wavelength. The values along a
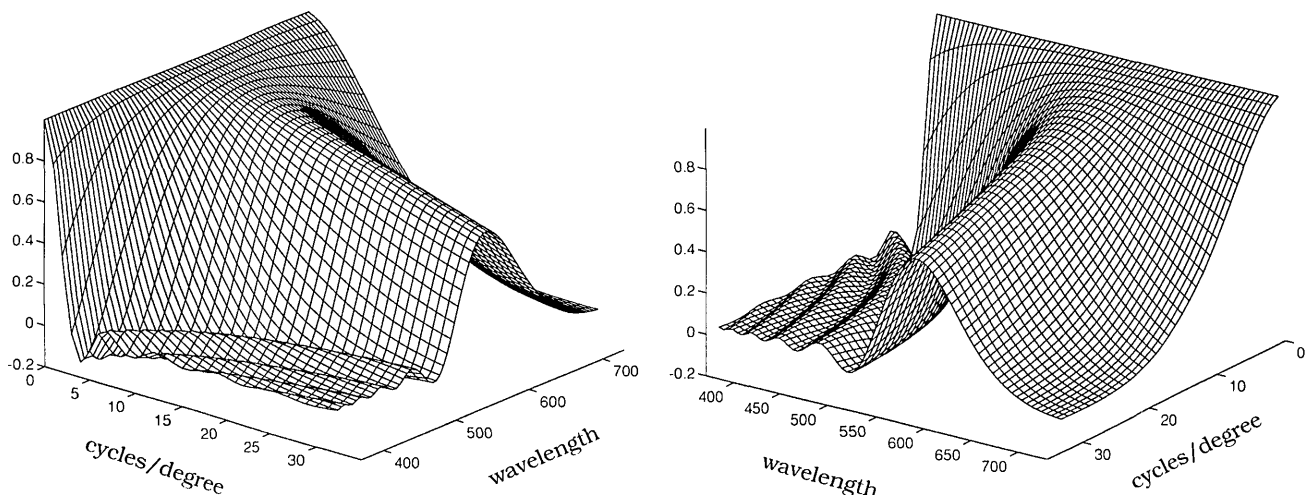

Fig. 2.   Two views of the OTF of the model eye with a pupil diameter of 3.0 mm.

single wavelength value define the one-dimensional OTF of a diffraction-limited optical system with the same chromatic defocus as that of human optics. The values along a single spatial-frequency value define the wavelength transfer function of the model eye at that spatial frequency. The OTF shown is based on a 3.0-mm pupil diameter.

Except at low spatial frequencies, only the band of wavelengths near the in-focus wavelength contributes significant contrast to the image. As Fig. 2 shows, this band becomes narrower as spatial frequency increases. The tendency toward monochromacy is present at all pupil diameters, but it is most dramatic for large pupil diameters.

B. Wavelength-Independent Aberrations

Although axial chromatic aberration is a major source of optical defocus, other aberrations contribute as well. To bring our analysis of the human retinal image into closer agreement with empirical observations, we use the results from Williams et al.[12] to describe the effects of wavelength-independent aberrations (also known as monochromatic aberrations). These authors measured the OTF of the human eye with interferometric and double-pass methods. In the absence of aberrations, the OTF of the human eye is diffraction limited at the in-focus wavelength. Because their stimulus was a monochromatic light and the observer's eye was in focus for the wavelength of that light, the difference between the observed and the diffraction-limited OTF's is an estimate of the effect of wavelength-independent aberrations. Williams et al. modeled the observed OTF as the product $O_d(\nu)K(\nu)$, where $O_d(\nu)$ is the diffraction-limited OTF at the relevant wavelength and $K(\nu)$ is a scale factor that reduces the diffraction-limited OTF at each spatial frequency. Hence the scale factor captures the effects of the wavelength-independent aberrations. Their estimate of the scale factor is

$$K(\nu) = 0.3481 + 0.6519 \exp(-0.1212\nu). \quad (5)$$

We can use the wavelength-independent scale factor $K(\nu)$ to estimate a combined OTF that incorporates both (axial) chromatic aberration and wavelength-independent aberrations. We obtain the combined OTF, denoted $O(\nu, \lambda)$, by multiplying the Hopkins OTF at every wavelength by the scale factor, as in

$$O(\nu, \lambda) = O_m(\nu, \lambda)K(\nu).$$

Figure 3 shows a surface plot of the combined OTF. The inset shows the relationship of the Hopkins OTF O_m at the in-focus wavelength, where it is diffraction limited, and the combined OTF O, derived with the expression of Williams et al.[12]

C. Line Spread

Figure 4 collects the line-spread function at each wavelength into a single surface plot. The dimensions of the surface plot are spatial position and wavelength. Figure 4 illustrates that short-wavelength light from a line source will spread roughly half a degree of visual angle across the retina. Because the point spread is circularly symmetric, it can be calculated from the line spread (see Goodman[14]).

D. Photopigment Absorptions Measured through the Optics

The photoreceptors that contain the photopigment within the eye form a discrete sampling grid. When we calculate a continuous pattern of photopigment absorptions, as in Eq. (6) below, we treat the photopigment as if it forms a continuous sheet within the eye. The continuous sheet calculation segregates image formation from photoreceptor spatial sampling; the spatial color matches that we compute do not depend on the photoreceptor sampling mosaics or image translations.

Chromatic aberration implies that the spectral responsivity of the receptor photopigment, measured through the optics, will vary with the spatial frequency of the stimulus. To see how this comes about, consider the following thought experiment. Suppose that we measure the spectral responsivity of the photoreceptors, using monochromatic sinusoidal targets imaged through the optics. We measure the photopigment absorption by drifting a monochromatic sinusoidal pattern and measuring the amplitude of the time-varying absorption rate.

When measured through the optics, the photopigment absorptions will depend on both the transmission through the optics and the spectral absorbance of the photopigment. The transmission through the optics depends on both the wavelength and the spatial frequency of the in-
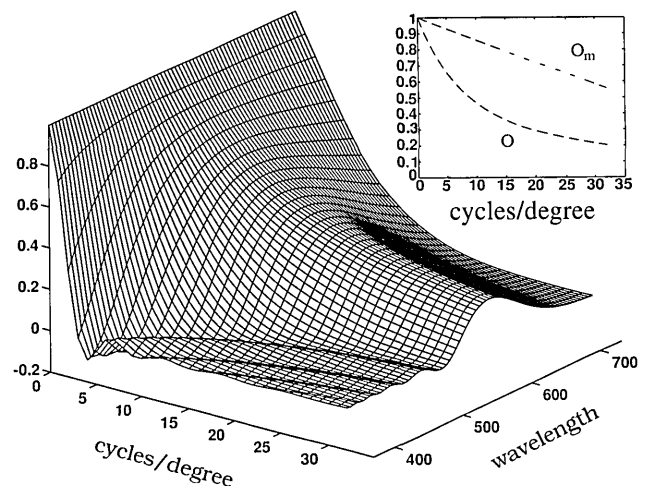

Fig. 3. OTF of the model eye, including wavelength-independent aberrations; upper panel, the Hopkins OTF (O_m) and the OTF including wavelength-independent aberrations (O) at the in-focus wavelength.
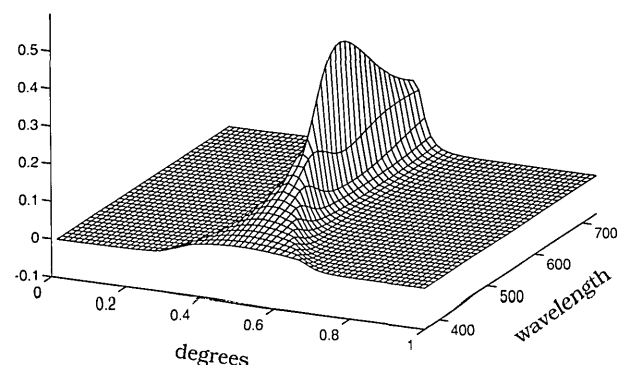

Fig. 4. Line spread of the model eye, including wavelength-independent aberrations.

put as described by the function $O(\nu, \lambda)$. Suppose that we call the absorption curves of the three photopigments $A_i(\lambda)$, $i = 1, 2, 3$. The photopigment absorption, measured through the optics, depends on both the spatial and the wavelength variables by the following definition:

$$R_i(\nu, \lambda) = O(\lambda, \nu)A_i(\lambda).$$

The function R_i generalizes the photopigment absorption curves A_i. Of course, the absorption curves of the photopigment molecules themselves are independent of spatial frequency. We propose this generalization because it is convenient for analysis and computation, but it applies only when the photopigment absorption curves are measured through the optics.

When we compute the photopigment absorptions P_i from a uniform field with spectral power distribution $F(\lambda)$, we use the formula

$$P_i = \int_W A_i(\lambda)F(\lambda)d\lambda,$$

where W is the range of visual wavelengths. But when we compute the Fourier transform of the spatial pattern of photopigment absorptions, $P_i(\nu)$, from an image with Fourier transform $F(\nu, \lambda)$, we replace the A_i with the functions that depend on spatial frequency R_i and use the formula

$$P_i(\nu) = \int_W R_i(\nu, \lambda)F(\nu, \lambda)d\lambda. \tag{6}$$

The plots in Fig. 5 illustrate how the photopigment absorption curves of the model eye, measured through the optics, vary as a function of spatial frequency. The surfaces in the left-hand column plot photopigment absorption as a function of stimulus wavelength and spatial frequency. The curves in the right-hand column plot the three cone responsivities at selected spatial frequencies. Chromatic aberration obliterates the short-wavelength cone response beyond a few cycles per degree. It also changes the shape and the peak value of the other two cone classes. When measured through the optics, the cone photopigment spectral responsivity depends strongly on the spatial frequency of the stimulus. Consequently, different spatial-frequency bands are encoded by use of sensors that have radically different color tuning.

The differences in the sensor absorbances at different spatial frequencies are so large that it is meaningless to compare the wavelength composition of spatial patterns at different spatial frequencies. The inability to compare wavelength information across spatial scale suggests a reason for the nervous system to select a multiresolution representation of image information. Photopigment absorption ratios within a spatial-frequency band are a meaningful measure of the spectral power distribution (SPD) of the incident light. But, because of chromatic aberration, comparison across spatial frequencies is not meaningful. Within a spatial-frequency band, comparisons of photopigment aborptions require, at least temporarily, a multiscale image representation.

4. APPLICATIONS

In this section we derive the procedure for creating photopigment absorption matches between two color images, using displays with different primaries.

The classic prediction of photopigment absorptions for large uniform areas expresses the relationship between display primary intensities and the photopigment absorptions, with use of a small matrix multiplication. If we group the three primary intensities into a column vector $\mathbf{m}$, there is a 3×3 matrix, $\mathbf{C}_0$, such that the product $\mathbf{C}_0\mathbf{m}$ equals the three photopigment absorptions to a spatially uniform field.

Because of chromatic aberration, this calculation does not generalize to point-by-point matches within an image. The generalization fails because the spatial pattern of photopigment absorptions depends on the wavelength composition of the point, making it impossible for one to set perfect matches by adjusting three primaries localized to a point.

We show that the correct generalization is to set matches in the spatial-frequency domain. [See Eq. (11) below.] Our result defines a simple procedure for matching the photopigment absorptions of images on displays with different emissive primaries. We define this matching procedure and then present examples of its use on different spatial patterns.

A. Displayed Image to Photopigment Absorptions

Conventional emissive displays have three primary lights, each with its own spectral power density. SPD's of typical CRT phosphors are shown in the left-hand panel of Fig. 6. The small number of primaries permits us to introduce some simplifications into the computation. We further simplify our derivations by considering one-dimensional images. Only the notation changes when we extend to two spatial dimensions.

At each spatial location the SPD of a one-dimensional image is a linear combination of the SPD's of the three primaries. We write this image as

$$f_m(x, \lambda) = \sum_{j=1}^{3} s_j(x)M_j(\lambda),$$

where $s_j(x)$ is the spatial image of the jth primary and $M_j(\lambda)$ is the SPD of the jth primary. The linearity of the Fourier transform permits us to transform both sides of this equation with respect to the spatial variable x. We write the Fourier-transform SPD of the input image as

$$F_m(\nu, \lambda) = \sum_{j=1}^{3} S_j(\nu)M_j(\lambda). \tag{7}$$

Here F_m and S_j are the Fourier transforms of f_m and s_j, respectively. The function F_m is a representation of the image in the Fourier domain.

We use Eq. (6) to compute the spatial pattern of photoreceptor responses by multiplying $R_i(\nu, \lambda)$ with the image F_m and then integrating with respect to wavelength:

$$P_i(\nu) = \int_W F_m(\nu, \lambda)R_i(\nu, \lambda)d\lambda. \tag{8}$$

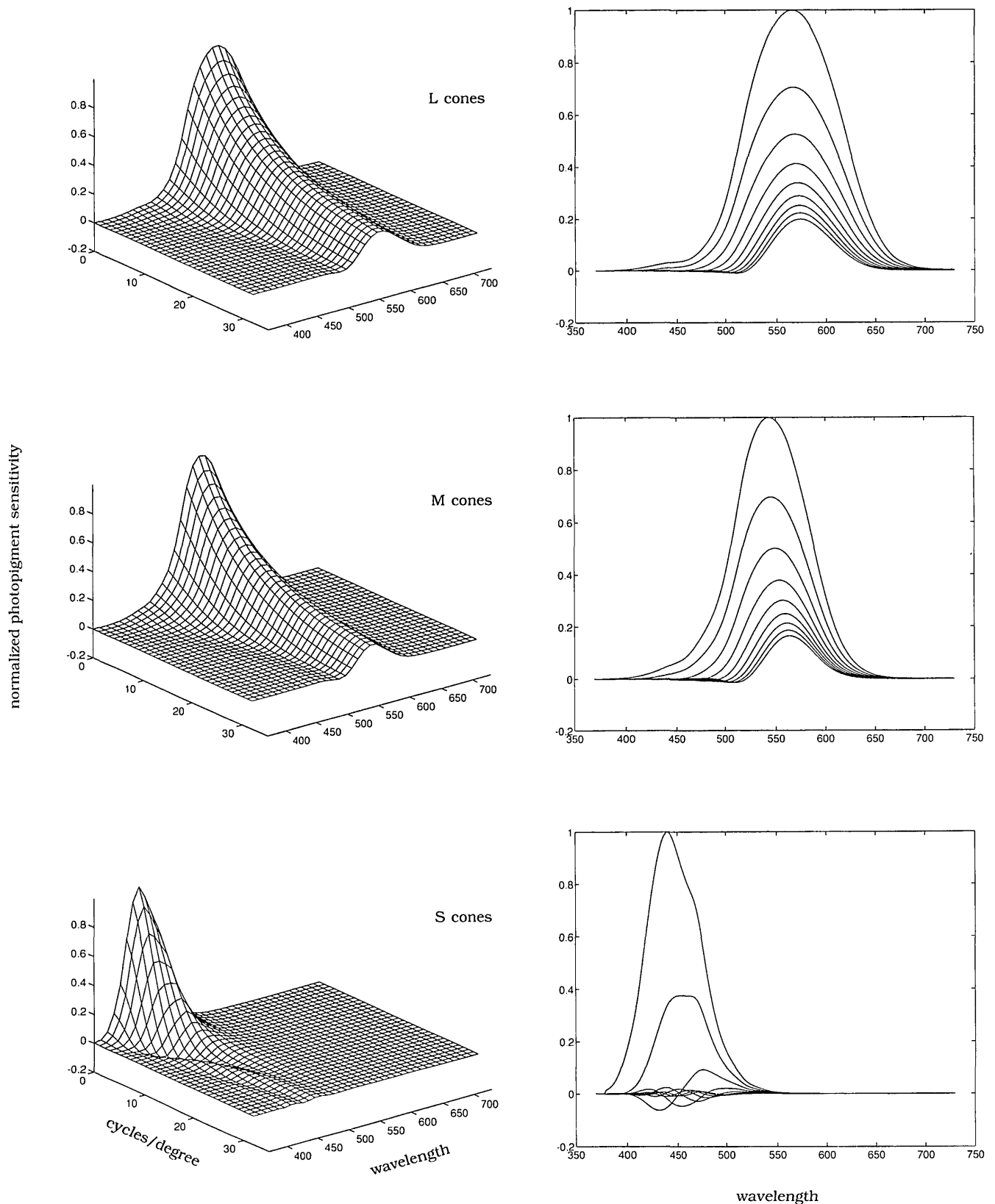The function $P_i(\nu)$ is the Fourier transform of the spa-

Fig. 5.   Cone photopigment sensitivities measured through the optics: in the left-hand column the surfaces define the sensitivity as a function of wavelength and spatial frequency; in the right-hand column the curves define the sensitivity as a function of wavelength, at spatial frequencies from 0 to 32 cycles/deg at intervals of 4 cycles/deg.   L, M, S: Long-, middle-, and short-wavelength, respectively.

tial pattern of photoreceptor responses for the ith class of cones and is based on the continuous sheet of photopigment described in Subsection 3.D.

It is convenient to express the integral in Eq. (8) in a slightly different form by substituting into it the definition of F_m from Eq. (7):

$$P_i(\nu) = \int_W \left[\sum_{j=1}^3 S_j(\nu)M_j(\lambda) \right] R_i(\nu, \lambda)\mathrm{d}\lambda$$

$$= \sum_{j=1}^3 S_j(\nu) \int_W M_j(\lambda)R_i(\nu, \lambda)\mathrm{d}\lambda .$$

The integral depends only on the spatial variable ν. Define a new function,

$$C_{ij}(\nu) = \int_W M_j(\lambda)R_i(\nu, \lambda)\mathrm{d}\lambda .$$

Using this notation, we can write the relationship between the spatial-frequency components of the three primary images and the spatial-frequency components of the spatial pattern of photoreceptors as

$$P_i(\nu) = \sum_{j=1}^3 C_{ij}(\nu)S_j(\nu). \tag{9}$$

The summation in Eq. (9) generalizes the matrix equation commonly used in color calibration with uniform spatial fields. We can write Eq. (9) as a matrix multiplication computed separately for each spatial-frequency component:

$$\begin{pmatrix} P_1(\nu) \\ P_2(\nu) \\ P_3(\nu) \end{pmatrix} = \begin{pmatrix} C_{11}(\nu) & C_{21}(\nu) & C_{31}(\nu) \\ C_{12}(\nu) & C_{22}(\nu) & C_{32}(\nu) \\ C_{13}(\nu) & C_{23}(\nu) & C_{33}(\nu) \end{pmatrix} \begin{pmatrix} S_1(\nu) \\ S_2(\nu) \\ S_3(\nu) \end{pmatrix}. \tag{10}$$

Equation (10) shows how to extend the relationship between display primary intensities and photopigment absorptions from the special case of a uniform field. When we incorporate the OTF into the calculation, we can relate the primary intensities to the photopigment absorptions by expressing the images in the spatial-frequency domain. We must use a different matrix at each spatial frequency.
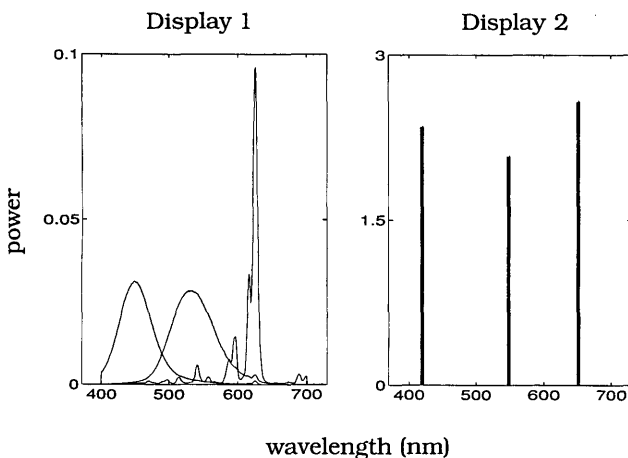

Fig. 6. Left, the SPD's of a typical CRT's phosphors; right, SPD's of a display based on three laser primaries selected to produce a large color gamut.

The entries of the matrix are determined by the SPD's of the display primaries, the receptor absorption functions, and the OTF of the eye.

We express the spatial-frequency-dependent matrix multiplication, using the matrix notation

$$\mathbf{P}_\nu = \mathbf{C}_\nu \mathbf{S}_\nu , \tag{11}$$

where $\mathbf{P}_\nu$ is a three-dimensional column vector with entries $P_i(\nu)$, $\mathbf{C}_\nu$ is a 3×3 matrix with entries $C_{ij}(\nu)$, and $\mathbf{S}_\nu$ is a three-dimensional column vector with entries $S_i(\nu)$. We call the collection of matrices $\mathbf{C}_\nu$ the device calibration matrices.

Notice that matrix $\mathbf{C}_0$ defines the mapping from the display primary intensities of a uniform field (spatial frequency of zero) to the receptor responses. This 3×3 calibration matrix is widely used in conventional colorimetry.[15-17] The device calibration matrices, which now depend on spatial frequency, generalize conventional colorimetric mapping from uniform fields to patterned images.

B. Image Matching across Displays

Using Eq. (11), we can develop a method of equating the photopigment absorptions from images on displays with different primaries. Suppose that we have two displays with calibration matrices $\mathbf{C}_\nu$ and $\mathbf{C}_\nu'$. Consider an image $\mathbf{S}_\nu$. We can calculate the expected pattern of photopigment absorptions for the image on the first display from the matrix multiplication $\mathbf{C}_\nu \mathbf{S}_\nu$. To equate photopigment absorptions from the two images requires that we find an image on the second display, defined by $\mathbf{S}_\nu'$ such that, at each spatial frequency,

$$\mathbf{C}_\nu' \mathbf{S}_\nu' = \mathbf{C}_\nu \mathbf{S}_\nu . \tag{12}$$

For each spatial frequency ν we can solve for the image $\mathbf{S}_\nu'$, using

$$\mathbf{S}_\nu' = (\mathbf{C}_\nu')^{-1}\mathbf{C}_\nu \mathbf{S}_\nu .$$

In practice we may be limited in how closely we can obtain the matches, because the matrices $\mathbf{C}_\nu'$ may not be invertible, and the solutions may not lie within the color gamut of the second display.

C. Examples

We now calculate the significance of chromatic aberration for color matching in several examples. Suppose that we wish to match images produced by a standard CRT, whose phosphors are shown in the left-hand panel of Fig. 6, and a display based on a novel display technology, say, using laser primaries chosen to maximize the display's color gamut, whose SPD's are shown in the right-hand panel of Fig. 6. We have chosen the maximum intensities of the display primaries so that uniform fields of maximum intensity have equal effects on the photopigments; this is called equating the display white points.

One way to see the effect of chromatic aberration is to calculate the spatial patterns of primary intensities on the second display that are needed to match simple
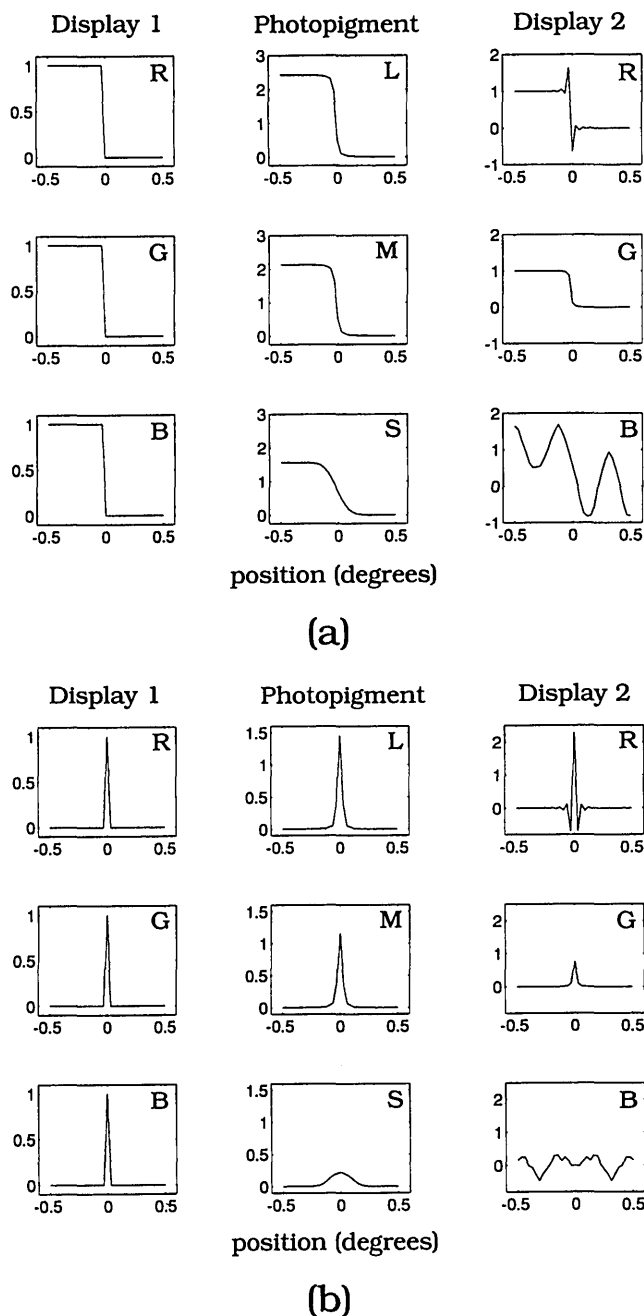
Fig. 7. Matching color images of (a) a step or (b) an impulse on two displays. The leftmost columns show the primary intensities of the pattern on the first display; the center columns, the resulting patterns of photopigment absorptions; and the rightmost columns, the primary intensities on the second display that produce the same patterns of photopigment absorptions, thereby matching the first display: R, G, B: red, green, and blue, respectively; L, M, S: long, middle, and short wavelength, respectively.

patterns, such as a step or an impulse, that are presented on the first display. In Fig. 7(a) the leftmost column of panels shows the primary intensities of a step from white to black on the first display, the middle column shows the corresponding photopigment absorptions for the three cone classes, and the rightmost column shows the primary intensities on the second display that are required for production of that pattern of photopigment absorptions. These absorptions are based on the continuous-sheet

calculation described in Subsection 3.D. Figure 7(b) is similar, except that the spatial pattern of primary intensities on the Display 1 is an impulse instead of a step.

The images on the two displays match because they produce the same pattern of photopigment absorptions. Chromatic aberration requires that we base our adjustment of the second display's primary intensities not only on the first display's primary intensities at the corresponding locations but on the spatial pattern of the primary intensities, as well.

For practical image matching it is important to correct for chromatic aberration in the range of up to 8 or 10 cycles/deg. Above this spatial-frequency value, patterns appear to be light and dark variations, no matter what their spectral composition.[18] Moreover, contrast resolution is so poor that there is little point in correcting even for contrast differences in the high-frequency range.[19]

5. RELATED RESEARCH

We have relied on a number of sources in our analysis and calculations. We summarize these here, and we draw the reader's attention to some related research.

Our basic model is due to Hopkins,[4] who derived the OTF of a defocused optical system with a circular aperture. Hopkins's analysis is also the basis of recent calculations by Flitcroft[13] and Williams et al.[20] The paper by van Meeteren[7] provides an extensive and general discussion of optical aberrations and parameters of the human eye. Legge et. al.[5] describe the relationship between optical defocus and the parameters necessary for implementing the Hopkins calculation.

Thibos et al.[9] recently developed a model of image formation in the human eye. Their research refers to many other models and data of the eye's image-formation properties that are beyond the scope of our analysis. These papers explore model eyes that include effects such as spherical aberration (e.g., Thibos et al.[21]) and transverse chromatic aberration (e.g., Simonet and Campbell[22]) that are not shift invariant. We have used the Thibos et al.[9] prediction of axial chromatic aberration, which in turn follows LeGrand.[23] Their model is linear but not shift invariant. Additional precision in the image-formation model may arise from a consideration of the general class of linear models. The theoretical simplicity of our results, however, depends on the use of a shift-invariant linear model of image formation. We have adopted the simpler version so that we can obtain closed-form approximations. We suspect that over the central 2 deg of vision, where the role of color is most significant, the shift-invariant model will play a useful role.

Finally, the indispensable volume by Wyszecki and Stiles[3] contains many additional references and human-eye parameters.

6. CONCLUSIONS

To calculate the photopigment absorptions of a patterned stimulus, we must include the effects of the image-formation components on the optical path prior to the photopigments. Many of the components, such as inert pigments, have the same effect on all corneal images.

Chromatic aberration is somewhat more complex, because its effects are pattern dependent.

We have explored the implications of chromatic aberration for color matching with patterned stimuli. Our analysis is based on a shift-invariant linear model of the human eye that includes diffraction, chromatic aberration, and wavelength-independent aberrations. Our model eye includes many specific and somewhat arbitrary assumptions about practical viewing conditions. For example, our calculations are based on a 3.0-mm pupil size and an accommodated wavelength of 580 nm. Still, the central conclusions of our analysis will hold for any human eye for which a shift-invariant linear system is a good model. Three conclusions stand out from our analysis.

First, above 20 cycles/deg only wavelengths near the accommodated wavelength can have detectable contrast in the retinal image (see Fig. 2). Even if the retinal contrast in this narrow band of wavelengths is detectable, the dynamic range of the visible contrast will be small. These two limitations imply that high-spatial-frequency components play little role in color and contrast perception. Rather, these components can aid us only in localization.

Second, in the moderate-spatial-frequency range, from 5 to 20 cycles/deg, when the observer is accommodated to the yellow or the green part of the spectrum, the visual system is dichromatic: there is no contrast in the short-wavelength receptor class. Moreover, across this spatial-frequency range, the spectral sensitivities of the long- and the middle-wavelength receptors vary with spatial frequency (see Fig. 5). Hence contrast and color comparisons are meaningful only within relatively small spatial-frequency ranges.

Third, we have shown that the conventional method of setting point-by-point matches between images fails to account for the fact that image points on different displays may not have the same line-spread (or point-spread) function on the retina. Since the spatial patterns on the retina from individual points on the displays do not match, one cannot match the retinal images of two points simply by adjusting the intensities of the three display primaries. To the extent that human image formation is linear and shift invariant, sinusoidal patterns in a display image remain sinusoidal in the retinal image. Since the spatial patterns from sinusoidal patterns do match, one can match the retinal images of two sinusoids simply by adjusting the intensities of the three display primaries. Hence to equate photopigment absorptions between images on different displays, one must adjust the primary intensities in the corresponding spatial-frequency bands.

APPENDIX A: HOPKINS'S OPTICAL TRANSFER FUNCTION INTEGRATED IN CLOSED FORM

Hopkins[4] found the following closed-form expression for the integral in Eq. (1):

$$H(s; \lambda, w_{20}) = \frac{4}{\pi a} \left[\left(\cos \frac{a|s|}{2} \right) H_1(a, \beta) \right.$$

$$\left. - \left(\sin \frac{a|s|}{2} \right) H_2(a, \beta) \right],$$

where

$$\beta = \cos^{-1} \frac{|s|}{2},$$

$$H_1(a, \beta) = \beta J_1(a) + \frac{\sin 2\beta}{2} [J_1(a) - J_3(a)] - \frac{\sin 4\beta}{4}$$

$$\times [J_3(a) - J_5(a)] + \dots,$$

$$H_2(a, \beta) = (\sin \beta)[J_0(a) - J_2(a)] + \frac{\sin 3\beta}{3} [J_2(a) - J_4(a)]$$

$$- \frac{\sin 5\beta}{5} [J_4(a) - J_6(a)] + \dots.$$

APPENDIX B: CONVERTING FROM REDUCED SPATIAL FREQUENCY TO CYCLES PER DEGREE

In this appendix we derive Eq. (2), the relationship between cycles per degree ν and Hopkins's[4] reduced spatial frequency s:

$$s = c \frac{\lambda}{D_0 p} \nu.$$

We begin with Eq. (17) of Ref. 4, which relates reduced spatial frequency and cycles per unit length in the image R' as follows:

$$s = \frac{\lambda}{n' \sin \alpha'} R'. \tag{B1}$$

Here n' is the index of refraction in the image space and α' is the half-angle of the cone subtended by the exit pupil at the image point.

Let d be the exit pupil's distance behind the image principal plane. Let p' be the radius of the exit pupil and f' be the image focal length. Then

$$\sin \alpha' = \frac{p'}{f' - d}.$$

For LeGrand's full theoretical eye,[4] $f' = 22.2888$ mm, $d = 1.7743$ mm, and $n' = 1.336$.

If we now express $\sin \alpha'$ in terms of the radius of the entrance pupil p, a very simple result follows. Define the constant k to be the ratio of the size of the entrance and exit pupils, namely, $k = p'/p$. It follows that

$$\sin \alpha' = \frac{k}{f' - d} p.$$

For LeGrand's full theoretical eye, $k = 0.9204$. For this value and the above-cited values of f' and d,

$$\frac{k}{f' - d} = 0.04487.$$

For the human optical system this numerical value is identical to that of $1/f'$ to four significant digits. Therefore we can use the approximation

$$\sin \alpha' = \frac{1}{f'} p. \tag{B2}$$

Two more relationships are needed to complete the derivation. The first is the relationship between cycles per unit length and cycles per degree,

$$R' = c\nu,$$

where c is degrees per meter for the human eye [see

Table 2(2.4.1) of Ref. 3]. The second relationship is the definition of dioptric power,

$$D_0 = n'/f'.$$

Substituting for $\sin \alpha'$ and R' in Eq. (B1) and using this definition of dioptric power yields Eq. (B2).

APPENDIX C: CONVERTING FROM w_{20} TO DEFOCUS IN DIOPTERS

In this appendix we derive Eq. (3), which defines the relationship between defocus measured in diopters and path length error w_{20}:

$$w_{20}(\lambda) = \frac{p^2}{2} \frac{D_0 D(\lambda)}{D_0 + D(\lambda)}.$$

We begin with the definition of the focusing error w_{20} [Eq. (13) of Ref. 4]:

$$w_{20} = \frac{n'z}{2} \sin^2 \alpha', \qquad \text{(C1)}$$

where z is the axial distance from the out-of-focus image plane to the in-focus image plane. From Appendix B we know that

$$\sin \alpha' = p/f'.$$

By substituting for $\sin \alpha'$ in Eq. (C1) we obtain

$$w_{20} = \frac{n'z}{2} \left(\frac{p}{f'} \right)^2. \qquad \text{(C2)}$$

Recall the definition of dioptric power,

$$D_0 = n'/f',$$

so that

$$D_0 + D = \frac{n'}{f' - z}, \qquad \text{(C3)}$$

where D_0 is the baseline dioptric power of the eye. From these two equations we find that

$$z = \frac{n'D}{D_0(D_0 + D)},$$

$$f' = n'/D_0.$$

Substituting these expressions for z and f' in Eq. (C2) yields Eq. (C3), as is required.

ACKNOWLEDGMENTS

David H. Marimont's E-mail address is marimont@parc.xerox.com; Brian A. Wandell's E-mail address is brian@psych.stanford.edu.

REFERENCES AND NOTES

1. D. A. Baylor, B. J. Nunn, and J. L. Schnapf, "Spectral sensitivity of cones of the monkey *Macaca fascicularis*," J. Physiol. **390**, 145–160 (1987).
2. J. L. Schnapf, T. W. Kraft, and D. A. Baylor, "Spectral sensitivity of human cone photoreceptors," Nature (London) **325**, 439–441 (1987).
3. G. Wyszecki and W. S. Stiles, *Color Science: Concepts and Methods, Quantitative Data and Formulae*, 2nd ed. (Wiley, New York, 1982).
4. H. H. Hopkins, "The frequency response of a defocused optical system," Proc. R. Soc. London Ser. A **231**, 91–103 (1955).
5. G. E. Legge, K. T. Mullen, G. C. Woo, and F. W. Campbell, "Tolerance to visual defocus," J. Opt. Soc. Am. A **4**, 851–863 (1987).
6. G. Wald and D. R. Griffin, "The change in refractive power of the human eye in dim and bright light," J. Opt. Soc. Am. **37**, 321–336 (1947).
7. A. van Meeteren, "Calculations on the optical modulation transfer function of the human eye for white light," Opt. Acta **21**, 395–412 (1974).
8. R. E. Bedford and G. Wyszecki, "Axial chromatic aberration of the human eye," J. Opt. Soc. Am. **47**, 564–565 (1957).
9. L. N. Thibos, M. Ye, X. Zhang, and A. Bradley, "The chromatic eye: a new reduced-eye model of ocular chromatic aberration in humans," Appl. Opt. **31**, 3594–3600 (1992).
10. V. Smith and J. Pokorny, "Spectral sensitivity of the foveal cone photopigments between 400 and 500 nm," Vision Res. **15**, 161–171 (1975).
11. R. M. Boynton, *Human Color Vision* (Holt, Rinehart & Winston, New York, 1979).
12. D. R. Williams, D. Brainard, M. McMahon, and R. Navarro, "Double-pass and interferometric measures of the optical quality of the eye," J. Opt. Soc. Am. A **11**, 3123–3135 (1994).
13. In D. I. Flitcroft, "The interactions between chromatic aberration, defocus, and stimulus chromaticity: implications for visual physiology and colorimetry," Vision Res. **29**, 349–360 (1989), a different approximation is used to describe this relationship. In Flitcroft's Fig. 1 (p. 350) he fits the same data, using the function $D = A - Bp^x$, where $x = (\lambda - 350)/50$, λ is wavelength in nanometers, $p = 0.7621$, $A = 0.8248$, $B = 3.5450$, and D is defocus in diopters. We replotted this equation and concluded that Flitcroft erred somewhere; this function does not pass through the data nearly so well as the curve illustrated in his figure.
14. J. W. Goodman, *Introduction to Fourier Optics* (McGraw-Hill, San Francisco, Calif., 1968).
15. D. H. Brainard, "Calibration of a computer-controlled color monitor," Col. Res. Appl. **14**, 23–34 (1989).
16. J. D. Foley, A. van Dam, S. K. Feiner, and J. F. Hughes, *Computer Graphics: Principles and Practice*, 2nd ed. (Addison-Wesley, New York, 1990).
17. B. A. Wandell, *The Foundations of Color Measurement and Color Perception*, Society for Information Display Lecture Notes (Society for Information Display, Santa Ana, Calif., 1992).
18. A. B. Poirson and B. A. Wandell, "The appearance of colored patterns: pattern–color separability," J. Opt. Soc. Am. A **10**, 2458–2471 (1993).
19. J. M. Foley and G. E. Legge, "Contrast detection and near-threshold discrimination in human vision," Vision Res. **21**, 1041–1053 (1981).
20. D. R. Williams, N. Sokiguchi, W. Haake, D. Brainard, and O. Packer, "The cost of trichromacy for spatial vision," in *From Pigments to Perception*, A. Valberg and B. B. Lee, eds. (Plenum, New York, 1991), pp. 11–22.
21. L. N. Thibos, A. Bradley, D. L. Still, X. Zhang, and P. A. Howard, "Theory and measurement of ocular chromatic aberration," Vision Res. **30**, 33–49 (1990).
22. P. Simonet and M. C. W. Campbell, "The optical transverse chromatic aberration on the fovea of the human eye," Vision Res. **30**, 187–206 (1990).
23. Y. LeGrand, *Form and Space Vision*, G. G. Heath and M. Millodot, transl. (Indiana U. Press, Bloomington, Ind., 1967).